M-2575

J. Chem. Thermodynamics **1991,** 23, 261–272

Thermodynamics of iron sulfides
I. Heat capacity and thermodynamic properties of Fe_9S_{10} at temperatures from 5 K to 740 K

FREDRIK GRØNVOLD, SVEIN STØLEN,

Department of Chemistry, University of Oslo, Blindern N-0315 Oslo 3, Norway

ABDUL K. LABBAN, and EDGAR F. WESTRUM, JR.

Department of Chemistry, University of Michigan, Ann Arbor, MI 48109, U.S.A.

(Received 9 October 1990)

Measurements of the heat capacity of Fe_9S_{10} over the temperature range 5 K to 740 K reveal a first-order structural transition at 495 K and two higher-order transitions with maxima at 534 K and 591 K. The last two are of coupled magnetic and structural origin. The structural changes giving rise to the heat-capacity effects are identified, and the magnetic properties are interpreted in terms of these. The standard entropy at 298.15 K of $(1/19)Fe_9S_{10}$ is compared with those of (1/2)FeS and $(1/15)Fe_7S_8$. The origin of the higher molar entropy for the first compound is found to reside mainly in the higher electronic heat-capacity contribution. The thermodynamic properties for $(1/10)Fe_9S_{10}$ have been evaluated and the values of $C_{p,m}$, $\Delta_0^T S_m^\circ$, and $\Delta_0^T H_m^\circ$ are $6.171 \cdot R$, $7.598 \cdot R$ and $1147.3 \cdot R \cdot K$ at 298.15 K and are $6.944 \cdot R$, $14.524 \cdot R$, and $4572.4 \cdot R \cdot K$ at 740 K. ($R = 8.31441\ J \cdot K^{-1} \cdot mol^{-1}$).

1. Introduction

Five different pyrrhotites have been ascertained as stable at room temperature.[1] In addition to FeS, the four compositions Fe_7S_8, Fe_9S_{10}, $Fe_{10}S_{11}$, and $Fe_{11}S_{12}$ are considered to be stoichiometric compounds. In the present paper heat-capacity results over the temperature range 5 K to 740 K are presented for one of these: Fe_9S_{10}.†

The structures of the pyrrhotites may be described as superstructures of the hexagonal NiAs-type structure, created by alternate stacking of filled and ordered defective iron layers normal to the *c*-axis.[2] Each structure is characterized by a well-defined ordered stacking of such layers, leading to the different superstructures.[3,4] The structure of Fe_9S_{10} is denoted 5*C*, and has a hexagonal cell with

† The portion of this work done at the University of Oslo is in part based on the cand. real. thesis of A. Langen (deceased).

0021–9614/91/030261+12 $02.00/0

a-axis equal to $2A$ and *c*-axis equal to $5C$ where A and C refer to the cell edges of the NiAs type structure. Although the $5C$ type is commonly found in nature, synthetic crystals of this type have not been obtained. According to Nakazawa and Morimoto[2] their synthetic Fe_9S_{10} was characterized by $c = NC$ with $N = 4.7$ at room temperature and $N = 4.2$ at 485 K. The low-temperature antiferromagnetic properties of Fe_9S_{10} have been interpreted in terms of two negatively coupled sublattices with a resulting net balance of vacancies.[5] The continuously decreasing periodicity along the *c*-axis may originate from stacking of $5C$ and $4C$ structural elements leading to an intermediate non-commensurate *c*-axis,[2] in analogy with the incommensurate superstructures of low digenite.[6]

The $5C$ structure transforms near 485 K into one with an incommensurate *a*-axis.[2] This NA type structure is described by $a = NA$ and $c = 3C$, where $N = 43$ at 485 K and $N = 90$ at 563 K.[2] The transformation process is limited by mass transport—*i.e.* vacancy rearrangements—according to Marusak and Mulay,[7] with an equilibration time of about 1 h. Lotgering[8] interpreted the ferrimagnetism as a result of a competition between spin- and vacancy-ordering. Andresen and Torbo[9] showed that this model was incorrect by proving that the spins remain ordered up to the Néel temperature. The ferrimagnetic structure, which originates from an uneven distribution of vacancies in different layers—with ferromagnetic coupling within a layer and antiferromagnetic coupling between neighbouring layers[5]—transforms back into an antiferromagnetic NiAs-type structure around 530 K. The transformation reflects changes in the stacking sequences or in magnetic coupling. Fe_9S_{10} is magnetically disordered above 590 K.

No prior heat-capacity determinations exist for Fe_9S_{10}.

2. Experimental

The iron sulfides were prepared directly from the elements. The iron was in the form of a continuous rod, 99.998 mass per cent pure, from the Koch-Light Laboratories, Ltd., Colnbrook, England. The sulfur was 99.9999 mass per cent pure crystals from the same manufacturer. The mixture of the elements was heated in an evacuated and sealed vitreous silica tube, constricted in the middle by a small-diameter tube. Iron was placed in one part of the tube and sulfur in the other, and the tube was put into an inclined tube furnace with the sulfur-containing compartment protruding upwards. The iron was heated to 970 K and the sulfur was allowed to melt and flow into the hotter part of the tube. When most of the sulfur had combined with the iron, a heating pad was wound around the exterior end of the silica tube. Thus, the remaining sulfur was brought into reaction overnight. The empty half of the silica tube was sealed off and discarded before annealing the sample, first at 1270 K for 3 h, then at 560 K for 30 d. The sample was finally crushed and transferred to the calorimetric ampoule. The characterization of the sample was made by powder X-ray diffraction.

The cryogenic calorimetric measurements were made in the Mark XIII cryostat described previously,[10] using intermittent heating adiabatic equilibrium methods. The programming, data logging, and calorimetry were computerized as described

elsewhere.[11] A gold-plated copper calorimeter (designated W-AB) was loaded with 131.97 g of Fe_9S_{10}. The buoyancy correction was calculated on the assumed density of 4.66 $g \cdot cm^{-3}$. Following evacuation, the pressure 2.7 kPa of purified helium was added to the calorimeter to enhance thermal equilibration. The calorimeter was then sealed in a vacuum chamber *via* a screw cap, which pressed a gold gasket against the circular knife edge on the stainless-steel neck of the calorimeter. All measurements of mass, resistance, potential, and time were referred to standardizations and calibrations performed at the U.S. National Bureau of Standards.

The higher-temperature calorimetric apparatus and measuring technique have been described earlier.[12] The calorimeter was intermittently heated, and surrounded by electrically heated and electronically controlled adiabatic shields. A mass 132.09 g Fe_9S_{10} was enclosed in an evacuated sealed silica-glass tube of about 50 cm^3 volume, tightly fitted into the silver calorimeter. A central well in the tube served for the heater and platinum resistance thermometer. The platinum resistance thermometer was calibrated locally, at the ice, steam, tin, and zinc points. Temperatures are judged to correspond with IPTS-68 to within 0.08 K.

The heat capacity of each empty calorimeter was determined in a separate series of experiments. It was, for the low-temperature calorimetric experiments, 9 per cent of the total at 5 K, 18 per cent at 50 K, and 16 per cent above 300 K. For the higher-temperature experiments the heat capacity of the empty calorimeter was about 50 per cent of the total, except in the transitional regions.

Room temperature X-ray powder photographs were taken in a Philips diffractometer with Cu $K\alpha_1$ radiation, and Si as internal calibration substance, a(293 K) = 543.1065 pm.[13] Low- and high-temperature X-ray photographs were obtained at temperatures between 90 K and 750 K in an Enraf–Nonius (FR 553) Guinier–Simon camera described earlier.[14] Unit-cell dimensions were derived by applying the program CELLKANT.[15]

3. Results and discussion

STRUCTURAL PROPERTIES

The unit-cell dimensions at room temperature, $a = (688.8 \pm 0.3)$ pm and $c = (2865.8 \pm 3.6)$ pm, are in good agreement with earlier reported values by Carpenter and Desborough[16] ($a = 689.2$ pm, $c = 2863.0$ pm, and $a = 688.4$ pm, $c = 2861.0$ pm for Fe_9S_{10} from two different locations) and by Morimoto *et al.* {$a = (688.83 \pm 0.10)$ pm, $c = (2867.00 \pm 0.15)$ pm;[17] and $a = (688.48 \pm 0.14)$ pm, $b = (1194.36 \pm 0.06)$ pm, and $c = (2867.60 \pm 0.15)$ pm, using an orthorhombic setting}.[18]

In figure 1, the unit-cell dimensions of the basic NiAs-type cell are given as a function of temperature. These values are based on the main reflections only. The superstructure reflections are very weak and could not be used for evaluation of the variation in the superstructure cell dimension with temperature. At higher temperatures the NiAs-type structure prevails. These observations are in good agreement with those by Nakazawa and Morimoto.[2]

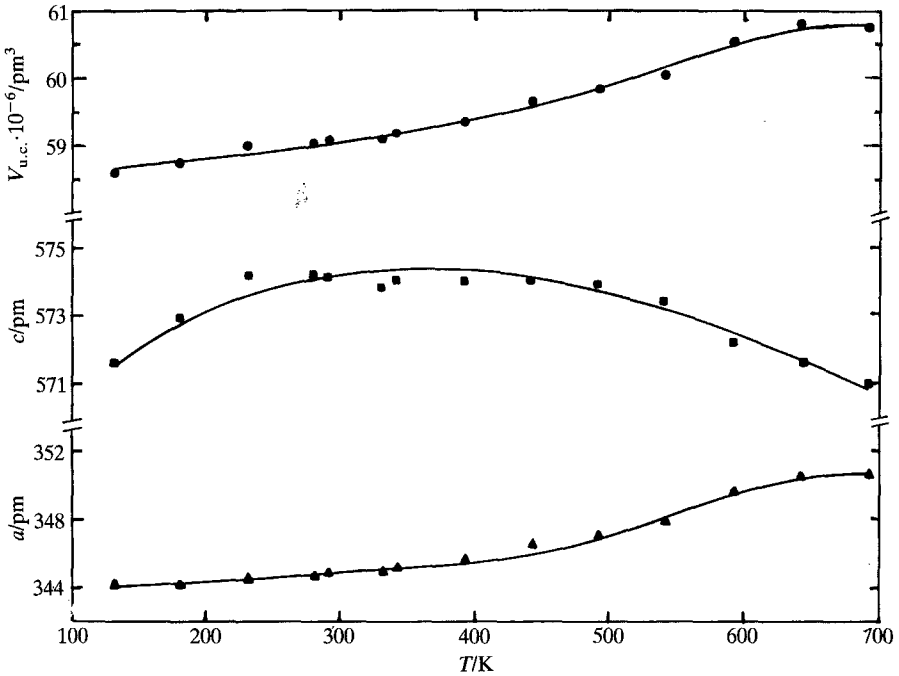

FIGURE 1. Unit-cell dimensions of the NiAs-type subcell of Fe_9S_{10} as a function of temperature.

The mean thermal expansivity for Fe_9S_{10} is $4.5\cdot10^{-5}$ K^{-1} over the temperature range 300 K to 700 K, in reasonable agreement with earlier results for $Fe_{0.893}S$.[19] Corresponding values for FeS and for Fe_7S_8 are $8.7\cdot10^{-5}$ K^{-1} ($294 < T < 393$ K)[20] and $4.5\cdot10^{-5}$ K^{-1} ($298 < T < 414$ K),[21] and $1.9\cdot10^{-5}$ K^{-1} ($80 < T < 300$ K),[22] respectively.

HEAT CAPACITY

The experimental heat capacities for $(1/10)Fe_9S_{10}$ from both low- and high-temperature ranges, are listed in chronological order for the mean temperatures in table 1 and presented graphically in figure 2. The approximate temperature increments used in the determinations can usually be inferred from the adjacent mean temperatures in table 1.

Twice the standard deviation in the measured low-temperature heat capacity is about 1 per cent from 8 K to 10 K, 0.3 per cent from 10 K to 30 K and 0.1 per cent from 30 K to 350 K. In the higher-temperature range it is about 0.3 per cent.

TRANSITIONS

Fe_9S_{10} takes a randomized NiAs-like structure at high temperatures. Below a certain temperature the $T\cdot\Delta S$ increment due to randomized vacancies is smaller than the

TABLE 1. Experimental values of the heat capacity of $(1/10)Fe_9S_{10}$. ($R = 8.31441\ J \cdot K^{-1} \cdot mol^{-1}$; $M\{(1/10)Fe_9S_{10}\} = 82.3283\ g \cdot mol^{-1}$)

$\langle T \rangle$/K	$C_{p,m}/R$	$\langle T \rangle$/K	$C_{p,m}/R$	$\langle T \rangle$/K	$C_{p,m}/R$	$\langle T \rangle$/K	$C_{p,m}/R$	$\langle T \rangle$/K	$C_{p,m}/R$
High-temperature results—University of Oslo									
Series I		Series IV		597.42	8.495	528.46	10.434	370.37	6.712
302.09	6.284	493.29	9.980[a]	602.02	8.187	531.43	10.713	382.81	6.813
313.81	6.231	502.20	8.595	606.71	7.962	533.38	10.821	395.07	6.931
325.42	6.323	511.38	8.960	611.45	7.832	535.34	10.641	407.16	7.050
336.88	6.403	520.21	9.707	616.23	7.688	537.31	10.431	Series X	
348.17	6.514	528.62	10.449	623.48	7.527	540.35	10.006	617.76	7.452
Series II		536.87	10.280	Series VI[c]		Series VIII		629.11	7.422
368.97	6.690	545.32	9.617	462.86	7.688	418.04	7.138	640.51	7.322
379.82	6.832	553.94	9.544	475.83	7.873	429.82	7.271	651.96	7.224
390.49	6.893	563.26	9.633	483.43	8.134	441.43	7.369	663.45	7.156
401.05	6.979	573.18	9.836	485.78	8.323	452.89	7.538	674.98	7.096
411.47	7.091	582.91	10.242	488.11	8.290	464.17	7.697	686.54	7.093
421.78	7.202	Series V		490.45	8.221	475.28	7.877	698.08	7.094
431.96	7.299	570.93	9.795	492.77	8.412	486.20	8.094	Series XI	
Series III		580.67	10.121	494.55	19.61[b]	494.91	10.464[c]	703.61	6.989
438.94	7.375	587.48	10.672	496.31	8.631	Series IX		715.14	6.970
448.91	7.505	590.01	11.225	498.58	8.609	301.58	6.199	726.68	6.969
458.76	7.625	591.07	11.717	Series VII		315.07	6.287	738.21	6.957
468.49	7.758	592.15	10.431	513.91	9.101	328.35	6.369		
478.09	7.906	593.31	9.333	520.26	9.789	341.41	6.489		
487.55	8.079	594.53	9.039	524.43	10.064	354.28	6.568		
Low-temperature results—University of Michigan									
Series XII		20.57	0.244	53.57	1.589	131.73	4.119	238.66	5.616
5.38	0.0122	21.89	0.286	56.46	1.710	137.30	4.236	245.35	5.683
5.87	0.0143	23.23	0.330	59.55	1.837	142.88	4.351	252.04	5.744
6.59	0.0177	24.72	0.380	62.83	1.974	148.47	4.450	258.74	5.803
7.31	0.0193	26.33	0.441	66.32	2.114	154.06	4.561	265.44	5.860
8.00	0.0256	27.95	0.501	70.01	2.257	159.67	4.658	272.13	5.931
8.70	0.0280	29.60	0.565	73.91	2.401	165.29	4.745	278.81	6.002
9.49	0.0356	31.26	0.634	78.06	2.559	170.92	4.826	285.51	6.047
10.33	0.0427	32.92	0.705	82.45	2.725	176.80	4.909	292.20	6.117
11.19	0.0527	34.61	0.774	86.80	2.881	182.94	4.995	298.89	6.185
12.07	0.0625	36.40	0.850	91.43	3.033	189.08	5.081	305.86	6.234
12.93	0.0734	38.29	0.933	96.38	3.184	195.23	5.154	313.08	6.297
13.86	0.0884	40.18	1.015	101.34	3.336	201.39	5.232	320.30	6.355
14.90	0.107	42.19	1.099	106.33	3.477	207.56	5.290	327.51	6.414
15.93	0.128	44.29	1.192	111.34	3.615	213.71	5.366	334.72	6.466
16.99	0.151	46.40	1.284	116.35	3.746	219.88	5.432	341.95	6.529
18.05	0.176	48.49	1.374	121.39	3.872	226.05	5.490	347.74	6.564
19.24	0.207	50.87	1.480	126.43	3.997	232.23	5.548		

[a] $\Delta_{trs}H_m$ Determination A. [b] $\Delta_{trs}H_m$ Determination B. [c] $\Delta_{trs}H_m$ Determination C.

enthalpy increment of the less strongly bonded structure, and favors formation of superstructures.[23] Fe_9S_{10} transforms at 530 K to a so-called NA-type structure[24] and further structural rearrangements at 485 K lead to the room temperature 5C-type structure.[2] Other structural descriptions of the room-temperature structure

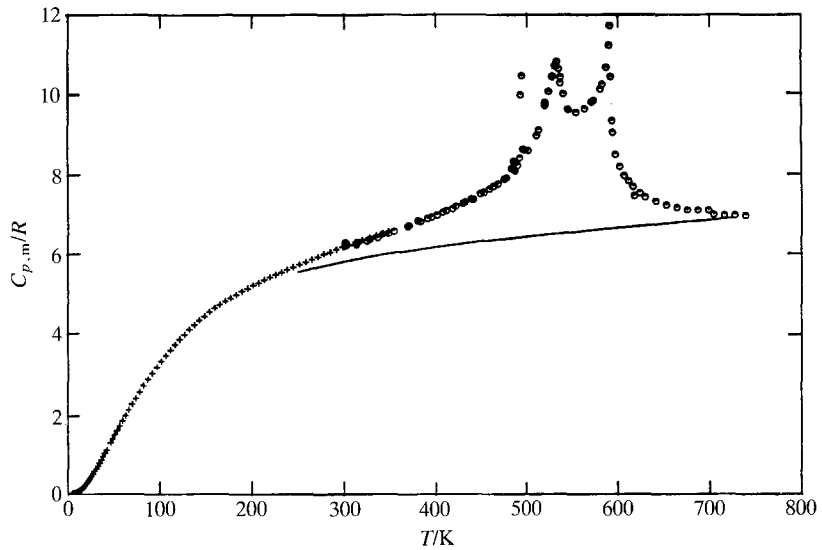

FIGURE 2. Molar heat capacity of (1/10)Fe_9S_{10}. +, U of M determinations; ⏲, U of O determinations; ——, the non-transitional molar heat capacity, see text.

exist.[3,25-27] A four-dimensional description of the *NC*-type structure, for all values of *N* and for any composition,[26] shows that the vacancies are concentrated on two or three successive sites in each row of Fe atoms along the *c*-axis. The interaction between the rows give rise to a spiral distribution of vacancies in analogy with that for 4*C*-type pyrrhotite, see Bertaut.[28] According to Nakazawa and Morimoto,[2] the value of *N* decreases continuously with increasing temperature to $T = 491$ K, where a sluggish transition to the *NA*-type takes place. The long time needed to obtain equilibrium magnetization[7] indicates a mass-transport limited process, *i.e.* vacancy rearrangement. The heat-capacity peak due to this transition at 494.6 K is rather narrow and the transitional entropy relatively small compared with the two higher-temperature transitions peaking at 534 K and 591 K, see figure 2 and tables 1 and 2. These two peaks reflect randomization of the vacancies and magnetic moments, respectively, giving rise to the high-temperature paramagnetic NiAs-type phase. The two lower-temperature structural transitions are also magnetic order-order transitions. At 494.6 K the antiferromagnetic phase changes to a ferrimagnetic one on heating, which again transforms back to the antiferromagnetic one around 534 K. Thus, a physically correct description of the energetics related to the disordering process implies a complex configurational model. If one assumes a pure order-disorder type transition, the maximum configurational entropy involves randomization of 1 vacancy on 10 iron positions, giving $\Delta_{trs}S_m(\text{structural}) = 0.33 \cdot R$ for (1/10)Fe_9S_{10}. This structural entropy increment represents disordering of a completely ordered structure, and is, hence, a maximum value. The magnetic entropy increment related to total randomization of the magnetic moments on the iron atoms is similarly $\Delta_{trs}S_m(\text{magn.}) = (9/10) \cdot R \cdot \ln(2S+1) = 1.46 \cdot R$, in the spin-only approximation of Fe^{2+} with $S = 2$.

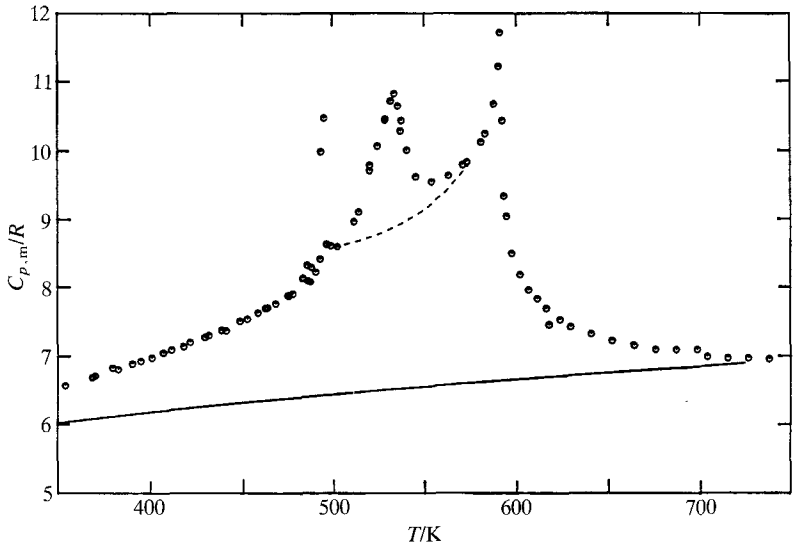

FIGURE 3. Deconvolution of the molar heat capacity of (1/10)Fe_9S_{10}. ⊙, Experimental molar heat capacity; – – –, "magnetic" reference molar heat capacity based on the molar heat capacity of FeS; ——, reference non-transitional molar heat capacity: $C_{ref,m} = C_{V,m} + C_{e,m} + C_{d,m}$.

A resolution of the excess heat capacity into contributions from the different structural and magnetic transitions is rather complicated. First of all, no method exists for accurate calculation of the background heat capacity. Using the thermodynamic quantities in table 4, a constant-volume heat capacity can be calculated, and from dilation and electrical conductivity additional heat-capacity contributions can be evaluated. The sum of these three contributions is, however, larger than the observed heat capacity at 740 K. Hence, the non-transitional contribution must be adjusted in order that the experimental heat capacity is equal to or larger than the reference heat capacity at 740 K. Since the constant-volume and the dilational heat capacities are derived from experiments (assuming isothermal compressibility of Fe_9S_{10} as equal to that of FeS), the electronic heat capacity is clearly over-estimated in the free electron gas model. A linear temperature dependence of C_{el} is to be expected only for temperatures which are low with respect to the degeneracy temperature E_f/k of the electron gas. Assuming the density of states proportional to $E^{1/2}$, *i.e.* a parabolic band, the electronic heat capacity can be expressed as $C_{el} = \gamma(T/\mathrm{K}) - \gamma'(T/\mathrm{K})^3$, see Stoner.[29] Choosing γ so that the experimental and the non-transitional heat capacities are equal at 740 K means $\gamma' = 7 \cdot 10^{-10} \cdot R$. The thus obtained non-transitional heat capacity is indicated by the solid lines in figures 2 and 3.

Furthermore, a "magnetic" reference heat capacity for deconvolution of the two higher-temperature transitions can be obtained using FeS as a reference. For this compound the high-temperature transition should be a purely magnetic transition from an antiferromagnetic to a paramagnetic state, without interference of any structural change. In this estimation scheme, the heat capacity of (1/2)FeS has to be

TABLE 2. $\Delta_{trs}H^{\circ}_{m}$ determinations for the 494.6 K transition in $(1/10)Fe_9S_{10}$. ($R = 8.31441\ J \cdot K^{-1} \cdot mol^{-1}$)

Detn.	$\langle T \rangle$ / K	$C_{p,m}/R$	$C_{p,m}(n.t.)/R$	T_i / K	T_f / K	$\Delta_{trs}H^{\circ}_{m}/R \cdot K$
A	493.29	9.980	8.26	489.036	497.546	14.6
B	494.55	19.61	8.30	493.922	495.185	14.3
C	494.91	10.464	8.30	491.606	498.215	14.3

$T_{trs} = (494.6 + 0.6)\ K \quad \Delta_{trs}S_m = (0.0290 \pm 0.0006) \cdot R \quad \Delta_{trs}H_m = (14.4 \pm 0.2) \cdot R \cdot K$

adjusted to equal that for $(1/19)Fe_9S_{10}$ at 740 K. The obtained resolution of the heat capacity is indicated in figure 3 (see also figure 2 for the reference non-transitional heat capacity). The heat-capacity increment of the lower-temperature transition is presumably superimposed on the increments from the two more gradual transitions. The derived entropy increments for transitions I (*5C*- to *NA*-type, antiferromagnetic to ferrimagnetic), II (*NA*- to NiAs-type, ferrimagnetic to antiferromagnetic), and III (antiferromagnetic to paramagnetic) for $(1/10)Fe_9S_{10}$ are $0.0290 \cdot R$, $0.134 \cdot R$, and $1.41 \cdot R$, respectively. The entropy increments for transition I for three different determinations are given in table 2. If we assume that the two magnetic order-order transitions result from vacancy rearrangements only, the total structural disordering entropy is $0.163 \cdot R$, whereas the corresponding magnetic entropy is $1.41 \cdot R$. Hence, the total disordering entropies are in reasonable agreement with those calculated above, using crude estimation schemes. The evaluated magnetic disordering entropy agrees very well, whereas the structural configurational entropy is only half of that expected from disordering of 1 vacancy on 10 iron positions. The deconvolution of the three transitions is, however, questionable and a slightly lower background heat capacity will give a considerably larger structural disordering entropy. It should also be noted that Keller-Besrest and Collin[21] report a gradual weakening of the superstructure reflections of the low-temperature structure of FeS with origin in a gradual disordering of vacancies even far below the transition temperature for the more cooperative disordering transformation.

THERMODYNAMIC PROPERTIES

The experimental heat capacities for the low- and high-temperature series were fitted to polynomials in temperature by the method of least squares. The fitting and especially the joins between the fitted segments were checked by inspection of plots of $dC_{p,m}/dT$ against T. The polynomials were then integrated by Simpson's rule to yield values of the thermodynamic functions at selected temperatures presented in table 3. Within the transition regions the heat-capacity values were read from large-scale plots and the thermodynamic functions were calculated by integration of the curves. At the lowest temperatures the heat capacities were smoothed with the aid of a plot of $C_{p,m}/T$ against T^2 and the functions were evaluated by extrapolation of this function. From this plot γ {for $(1/10)Fe_9S_{10}$} was found to be $0.0016 \cdot R \cdot K^{-1}$, or $C_{p,m}/R = 0.0016(T/K) + 0.0000247(T/K)^3$.

TABLE 3. Thermodynamic properties of $(1/10)Fe_9S_{10}$. ($R = 8.31441\ J \cdot K^{-1} \cdot mol^{-1}$)

$\frac{T}{K}$	$\frac{C_{p,m}}{R}$	$\frac{\Delta_0^T S_m^\circ}{R}$	$\frac{\Delta_0^T H_m^\circ}{R \cdot K}$	$\frac{\Phi_m^\circ}{R}$	$\frac{T}{K}$	$\frac{C_{p,m}}{R}$	$\frac{\Delta_0^T S_m^\circ}{R}$	$\frac{\Delta_0^T H_m^\circ}{R \cdot K}$	$\frac{\Phi_m^\circ}{R}$
				$M\{(1/10)Fe_9S_{10}\} = 82.3283\ g \cdot mol^{-1}$					
5	0.011	0.009	0.024	0.004	360	6.629	8.803	1543.1	4.517
10	0.040	0.024	0.131	0.011	380	6.787	9.166	1677.3	4.752
20	0.228	0.098	1.305	0.033	400	6.972	9.518	1814.8	4.981
30	0.583	0.254	5.265	0.079	420	7.181	9.863	1956.3	5.206
40	1.006	0.478	13.183	0.148	440	7.399	10.203	2102.1	5.425
50	1.440	0.750	25.414	0.242	460	7.629	10.536	2252.3	5.640
60	1.856	1.049	41.912	0.351	480	7.935	10.867	2407.7	5.851
70	2.257	1.366	62.48	0.473	494.60	(8.304)[a]	11.110	2526.0	6.003
80	2.636	1.692	86.97	0.605	494.60	(8.304)[a]	11.139	2540.4	6.003
90	2.982	2.023	115.09	0.744	500	8.496	11.230	2585.8	6.059
100	3.296	2.353	146.50	0.888	520	9.633	11.583	2765.8	6.264
120	3.840	3.004	218.03	1.187	534	10.9	11.86	2910	6.41
140	4.292	3.631	299.50	1.492	540	10.00	11.972	2972.1	6.468
160	4.659	4.229	389.14	1.797	560	9.57	12.321	3164.1	6.671
180	4.957	4.796	485.40	2.099	580	11.22	12.664	3359.7	6.872
200	5.210	5.331	587.1	2.396	591	11.7	12.86	3476	6.98
220	5.431	5.838	693.6	2.685	600	8.307	13.000	3557.6	7.071
240	5.628	6.319	804.2	2.969	620	7.589	13.259	3715.5	7.266
260	5.816	6.777	918.6	3.244	640	7.313	13.495	3864.1	7.457
273.15	5.940	7.067	995.9	3.421	650	7.239	13.607	3936.8	7.551
280	6.004	7.215	1036.8	3.512	660	7.183	13.718	4008.9	7.644
298.15	6.161	7.598	1147.3	3.750	680	7.099	13.931	4151.7	7.826
300	6.176	7.639	1158.8	3.773	700	7.035	14.136	4293.0	8.003
320	6.334	8.040	1283.8	4.028	720	6.982	14.333	4433.1	8.176
340	6.484	8.428	1412.0	4.275	740	6.944	14.524	4572.4	8.345

[a] Values predicted on the assumption that the transition is isothermal.

The standard molar entropy of $(1/19)Fe_9S_{10}$ at 298.15 K, $3.999 \cdot R$, is larger than those of (1/2)FeS and $(1/15)Fe_7S_8$, $3.627 \cdot R$ and $3.895 \cdot R$, respectively.[31] The reason for this anomalous behaviour can possibly be understood when the observed entropy is resolved into contributions from the different physical properties of the materials. The result of an attempt to deconvolute the total entropy is given in table 4. Here, only the constant-volume and the conduction-electronic entropy contributions are listed, the dilational and the magnetic contributions being difficult to estimate. The dilational contribution can be calculated from experimental thermal expansivities and isothermal compressibilities. The reported expansivity values are not consistent and no determinations at low temperatures have been made. The dilational contribution, which necessarily approaches zero as the temperature is lowered is, however, most probably not very different for the different compounds as the observed expansivities and compressibilities are of similar magnitude. The explicit obtainment of magnetic entropy values is also difficult. The magnetic heat capacity is proportional to $T^{3/2}$ for ferrimagnetic substances, and to T^3 for antiferromagnetic ones.[30] Thus, contribution from ferrimagnetism in Fe_7S_8 is not easily separated from the electronic contribution, which is proportional to T. In addition, a transition

TABLE 4. Thermal expansivity α; isothermal compressibility κ; conduction-electron heat-capacity coefficient γ; Debye temperature Θ_D; conduction-electron-, constant-volume-, and the observed entropy at $T = 298.15$ K for (1/2)FeS, (1/19)Fe_9S_{10}, and (1/15)Fe_7S_8

Substance	$\alpha \cdot 10^6$ / K^{-1}	Ref.	$\kappa \cdot 10^{12}$ / Pa^{-1}	Ref.	$\gamma \cdot 10^3$ / $R \cdot K^{-1}$	Ref.	Θ_D / K	$\Delta_0^T S_e / R$	$\Delta_0^T S_V / R$	$\Delta_0^T S^\circ_{obs} / R$
(1/2)FeS	87	20	12[a]	20	0	31	384	0.00	3.38	3.627
	45	21	29[b]	20						
(1/19)Fe_9S_{10}	90	19			0.84	this	378	0.25	3.42	3.999
	45	this								
(1/15)Fe_7S_8	19	22			0	31	370	0.00	3.48	3.895

[a] Low-temperature phase. [b] High-temperature phase.

near 8 K further complicates the resolution of the ferrimagnetic contribution. For FeS and Fe_9S_{10}, on the other hand, the heat-capacity contributions from antiferromagnetism are implicitly included in their constant-volume heat capacities.

The constant-volume and the conduction-electronic contributions to the entropy at 298.15 K are calculated using the scheme for resolution of the heat capacity discussed above. It should be noted that the conduction-electronic entropy at

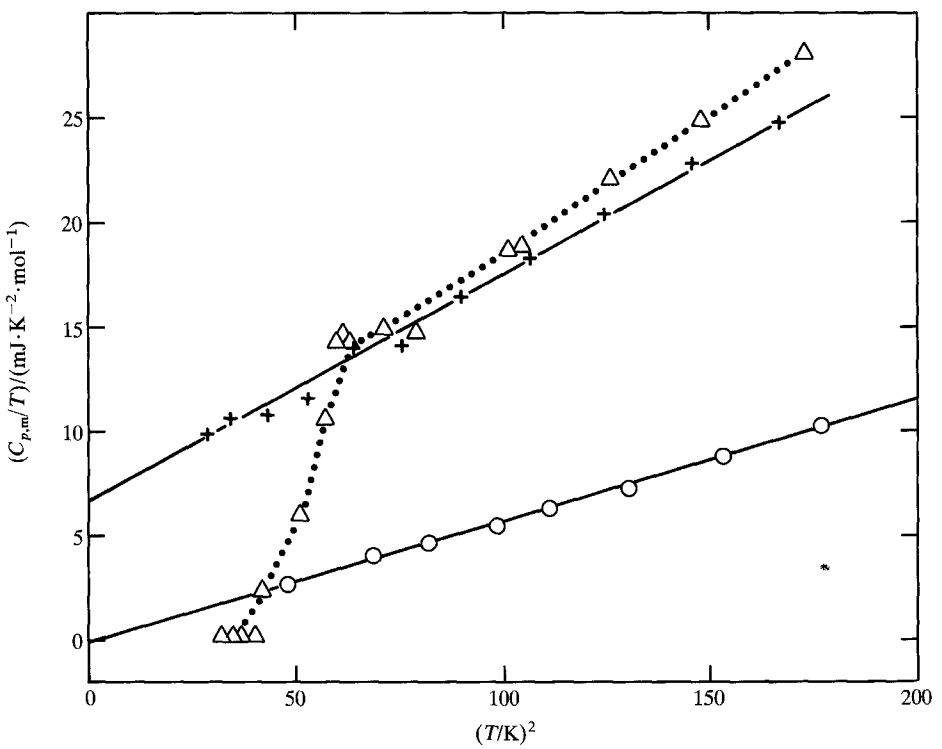

FIGURE 4. $C_{p,m}/T$ against T^2 at low temperatures. ○, (1/2)FeS;[31] +, (1/19)Fe_9S_{10}; △, (1/15)Fe_7S_8.[31]

298.15 K, calculated assuming a parabolic band, is only 2 per cent smaller than that calculated using the free-electron model.

Although the constant-volume molar entropy for (1/15)Fe_7S_8 is slightly larger than those for (1/2)FeS and (1/19)Fe_9S_{10}, the sum of the electronic and the constant-volume is much larger for the metallic conductor Fe_9S_{10}. The importance of the electronic contribution is thus substantiated. The residual entropies, *i.e.* S_{obs}-S_{el}-S_V, are, however, quite large. This is due to the neglect of any dilational and magnetic contributions (except what is incorporated in the lattice and conduction-electronic terms). In addition, the inadequacy of the Debye model may also cause systematic errors. The discrepancy is largest for Fe_7S_8. Here, an abrupt drop in the heat capacity at 8 K may indicate a metal-to-non-metal transition, see figure 4. A substantial conduction-electronic heat capacity can thus exist, even if it is impossible to resolve this contribution from the total observed heat capacity. An additional heat-capacity effect observed around 30 K,[31] which is due to a magnetic transition similar to the Verwey-transition,[32] further complicates the picture.

The portion of this work done at the University of Oslo was supported by the Norwegian Research Council for Science and the Humanities, whereas the portion done at the University of Michigan was supported by the Structural Chemistry and Chemical Thermodynamics Program, Division of Chemistry, National Science Foundation under grant No. CHE-771004.

REFERENCES

1. Morimoto, N.; Nakazawa, H.; Nishiguchi, K.; Tokonami, M. *Science* **1970,** 168, 964.
2. Nakazawa, H.; Morimoto, N. *Mater. Res. Bull.* **1971,** 6, 345.
3. Koto, K.; Morimoto, N.; Gyobu, A. *Acta Cryst.* **1975,** B31, 2759.
4. Power, L. F.; Fine, H. A. *Minerals Sci. Engng.* **1976,** 8, 106.
5. Schwarz, E. J.; Vaughan, D. J. *J. Geomagn. Geoelec.* **1972,** 24, 441.
6. Van Dyck, D.; Conde-Amiano, C.; Amelinckx, S. *Phys. Stat. Sol. (a)* **1980,** 58, 451.
7. Marusak, L. A.; Mulay, L. N. *Phys. Rev. B* **1980,** 21, 238.
8. Lotgering, F. K. *Philips Res. Rep.* **1956,** 190.
9. Andresen, A. F., Torbo, P. *Acta Chem. Scand.* **1967,** 21, 2841.
10. Westrum, E. F., Jr; Furukawa, G. T.; McCullough, J. P. *Experimental Thermodynamics, Vol. I.* McCullough, J. P.; Scott, D. W.: editors. Butterworths: London. **1968,** p. 133.
11. Westrum, E. F., Jr. *Proceedings NATO Advanced Study Institute on Thermochemistry.* Ribeiro da Silva, A. V.: editor. Reidel: New York. **1984,** p. 745.
12. Grønvold, F. *Acta Chem. Scand.* **1967,** 21, 1695.
13. Deslatters, R. D.; Henins, A. *Phys. Rev. Lett.* **1973,** 31, 972.
14. Grønvold, F.; Stølen, S.; Westrum, E. F., Jr.; Galeas, C. G. *J. Chem. Thermodynamics* **1987,** 19, 1305.
15. Ersson, N. O. Personal communication.
16. Carpenter, R. H.; Desborough, G. A. *Amer. Mineral.* **1964,** 49, 1350.
17. Morimoto, N.; Gyobu, A.; Mukaiyama, H.; Izawa, E. *Econ. Geol.* **1975,** 70, 824.
18. Morimoto, N.; Gyobu, A.; Tsukuma, K.; Koto, K. *Am. Mineral.* **1975,** 60, 240.
19. Grønvold, F.; Haraldsen, H. *Acta Chem. Scand.* **1952,** 6, 1452.
20. King, H. E., Jr.; Prewitt, C. T. *Acta Cryst.* **1982,** B38, 1877.
21. Keller Besrest, F.; Collin, G. *J. Solid State Chem.* **1990,** 84, 194.
22. Tsatis, D. E. *J. Phys. Chem. Solids* **1987,** 48, 489.
23. Stølen, S.; Grønvold, F. *J. Phys. Chem. Solids* **1987,** 48, 1213.
24. Nakazawa, H.; Morimoto, N.; Watanabe, E. *Electron Microscopy in Mineralogy.* Wenk, H. R., *et al.*: editors. Springer-Verlag: Berlin, Heidelberg. **1976,** p. 304.
25. Pierce, L. P.; Busek, P. R. *Science* **1974,** 186, 1209.

26. Yamamoto, A.; Nakazawa, H. *Acta Cryst.* **1982,** A32, 79.
27. Morimoto, N. *Recent Progr. Natural Sci. Japan* **1978,** 3, 183.
28. Bertaut, E. F. *Acta Cryst.* **1953,** 6, 557.
29. Stoner, E. C. *Phil. Mag.* **1935,** 21, 145.
30. Cracknell, A. P.; Tooke, A. O. *Contemp. Phys.* **1979,** 20, 55.
31. Grønvold, F.; Westrum, E. F., Jr.; Chou, C. *J. Chem. Phys.* **1959,** 30, 528.
32. Fillion, G.; Rochette, P. *J. Phys. Colloq.* **1988,** C8, 907.